

Intensification of iron-boron complex association in silicon solar cells under acoustic wave action

Oleg Olikh^{1*}, Vitaliy Kostylyov², Victor Vlasiuk², Roman Korkishko² and Roman Chupryna¹

¹Physics faculty, Taras Shevchenko National University of Kyiv, 64/13, Volodymyrska Street, Kyiv, 01601, Ukraine.

²V. Lashkaryov Institute of Semiconductor Physic of NAS of Ukraine, 41, pr. Nauki, Kyiv, 03028, Ukraine.

*Corresponding author(s). E-mail(s): olegolikh@knu.ua;

Contributing authors: vkost@isp.kiev.ua;

viktorvlasiuk@gmail.com; romkin.ua@gmail.com;

r_chupryna@voliacable.com;

Abstract

In this paper, we study the influence of ultrasound (US) on the recovery of light-induced degradation in Cz-Si solar cells. The complete recovery in the dark at near room temperature and the determined value of activation energy (0.656 eV) evidenced the iron–boron pair transformation-related degradation. The ability of extraction of FeB pair's parameters from short circuit current kinetics was discussed. It was revealed that the US loading leads to the acceleration of the FeB pair association. This effect was investigated for different US frequencies (0.3–30 MHz) and intensities (up to 1.3 W/cm²) as well as iron concentrations ((0.2–3) × 10¹³ cm^{−3}) in the solar cell over temperature range 300–340 K. It has been found that US longitudinal waves are more efficient than transverse waves. The experimentally observed phenomena are related to the decrease in iron migration energy (up to 10 meV) in the US stress fields.

Keywords: Ultrasound, Silicon solar cell, Iron-boron pair, Acousto-defect interaction

1 Introduction

It is well known that ultrasound (US) can act efficiently on defect subsystems of semiconductor crystals and devices due to dissipation of US vibration energy, which is particularly intense in the regions with periodicity disorder [1–3]. At US of **subthreshold** intensity, acoustically induced (AI) reconstruction of defects causes the **reversible** changes in charge concentration and mobility in crystals [4, 5], barrier height in Schottky structures [6, 7] as well as tunnel and recombination currents in p-n structures [3, 8]. Also, it seems promising to apply the US as an additional factor of influence during conventional technological processes. In this case, semiconductor structures are usually found in nonequilibrium conditions, and the defect–impurity subsystem is capable of modifying easier under the action of elastic oscillations. For instance, the application of ultrasound loading (USL) **during** ion implantation facilitates the formation of ultra-shallow junctions [9] and intensifies the silicon surface layer amorphization [10]; USL applied during the production of porous silicon results in structural ordering [11] and when applied during ZnO deposition provides higher homogeneity of the films [12].

The silicon solar cells (SCs) constitute about 90% of the global photovoltaic production capacity. Iron is one of the most relevant, omnipresent, and **efficiency-limiting** metallic impurities in p-type Si SCs [13, 14]. **Therefore, the methods of defect engineering aimed at iron have practical importance.** In silicon photovoltaics, one of the main methods of impurity deactivation and removing it from the operation zone is gettering Fe atoms at certain centers (extended defects, oxygen precipitates, or interfaces) [15]. A similar gettering can be realized during standard operations as phosphorus diffusion [16] or production of antireflection coating [17]. It is clear that the process efficiency depends on the mobility of iron atoms.

On the one hand, shallow acceptors (B, Al, Ga, In) are effective trapping sites for iron around room temperature and in darkness in p-Si due to electrostatic attraction between the negatively charged acceptors and the positively charged iron ions. All Fe-acceptor pairs are similar: complexes have two structural configurations with trigonal and orthorhombic symmetry and can be broken by intense illumination and/or annealing above 200°C [13, 18].

On the other hand, the back surface field (BSF) and passivated emitter and rear cell (PERC) are the most popular designs that have been used in the mass-production of Si SCs, and both BSF and PERC are mainly based on boron-doped silicon wafers [19, 20]. Therefore the iron–boron pair is one of the most relevant complexes to the defect engineering in real SCs. The aim of this work is to investigate experimentally how acoustic waves (AWs) influence the ability of iron to diffuse in silicon solar cells. The time of iron–boron pair association after light-induced dissociation was used as an indicator of iron ion mobility. The possibility of the ultrasound to change the state of FeB was shown previously [21, 22]. **In particular, the FeB pair was revealed [22] to be dissociated in Cz-Si by the action of ultrasound with acoustic strain $\xi_{\text{US}} = 10^{-5}$ – 10^{-4} . Furthermore, Ostapenko and Bell [22] regarded the**

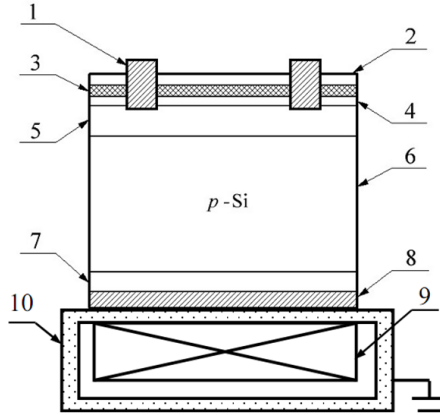


Fig. 1 Schematic structure of the sample and USL. 1 — frontal grid electrode (Al); 2 — Si_3N_4 (40 nm); 3 — SiO_2 (30 nm); 4 — induced n^{++} -layer; 5 — diffusion n^+ -layer; 6 — quasineutral base region of p -type (350 μm); 7 — diffusion p^+ -layer; 8 — rear metallization (Al); 9 — piezoelectric transducer; 10 — metal foil (Cu)

resonance condition of pair dissociation and used 25–70 kHz. Besides, it was asserted [21] that in the case of predominant dissociated pairs, the ultrasound may promote the pairing reaction in contradistinction to the case of a high fraction of paired iron. But empirical evidence for this prediction is absent. In this work, i) the $f_{\text{US}} = 2\text{--}30$ MHz and subthreshold strain $\xi_{\text{US}} < 2 \times 10^{-6}$ were used, which were deficient to effectively overcome the Coulombic attraction between Fe_i and B_s ; ii) the predominant dissociation of FeB was realized by intense illumination. Thus the association of FeB pair (the migration of Fe_i^+) was firstly investigated experimentally in conditions of USL.

2 Experimental and Calculation Details

Experimental studies were performed on the samples of silicon SC with geometric dimensions of 1.52×1.535 cm² made on the basis of single-crystal p -type silicon [100] wafers with resistivity of about 10 $\Omega\cdot\text{cm}$ (boron doping level $N_A = 1.4 \times 10^{15}$ cm⁻³). The thickness of the wafers was 380 μm . A diffusion from the gas phase (POCl_3) at 940°C was performed on wafers resulting in a n^+ -emitter layer on the front side (sheet resistance of about 20–30 Ω/\square , thickness of 0.7 μm). In addition, to reduce recombination losses and increase the conductivity of the contact layer, a p^+ layer (10–20 Ω/\square , 0.6 μm) was formed by boron diffusion from the gas phase (BCl_3) at 985°C on the rear surface. Layers of SiO_2 and Si_3N_4 were formed on the surface of the SC to passivate the surface and reduce optical reflectance. The solid and grid aluminum contacts were formed by magnetron sputtering on the rear and front surfaces, respectively. The schematic structure of SC is presented in Fig. 1.

In case of USL, the transverse or longitudinal AWs, which were excited by using LiNbO_3 or ceramic piezoelectric transducer, were applied to the samples

in [100] direction. The transducer was attached to the whole area of Al back contact. It is widely known that the efficiency of ultrasound influences defects in semiconductors depends on acoustic wave frequency f_{US} . Moreover, the type of frequency dependence is determined by the mechanism of acousto-defect interaction [23–25]. The set of longitudinal wave frequencies (2.4, 4.1, 5.4, 9.0, 14, 18, and 31 MHz) was used to establish features of ultrasound influence on iron migration. Besides, the effect of the increase in the carrier capture coefficient for defects in silicon SC is shown [26] to be intensified in the case of the transverse acoustic waves using. Accordingly, the transverse waves ($f_{\text{US}} = 0.3$ MHz) were used as well. The ultrasound intensities W_{US} does not overcome 1.3 W/cm^2 . To avoid the effect of the piezoelectric field on the measurements procedure as well as sample parameters, the transducer was shielded by Cu foil (see Fig. 1).

It is known that Fe in silicon can be in two states: in the form of FeB pair or in the interstitial state Fe_i . At near room temperature and boron concentration $> 10^{14} \text{ cm}^{-3}$, almost all Fe bound in FeB pairs is in equilibrium [27–30]. However, numerous researches show that dissociation of pairs can be performed either by heating to the temperature above 200°C , or by intense illumination at room temperature [28, 30]. In our work we used the latter approach, the lamp being used was a halogen lamp with radiation intensity of about 250 mW/cm^2 . To dissociate the pairs the frontal side of the sample was illuminated for 30 s.

The different light-induced degradation (LID) phenomena exist that affect the efficiency of Cz-silicon solar cells due to a decrease in lifetime of generated excess charge carriers. The main reasons for this transformation are boron–oxygen complex formation (BO-LID) [31] and iron–boron pair dissociation. Besides, the light- and elevated-temperature-induced degradation (LeTID) is observed. In recent studies the occurrence of the LeTID defect could be related to the presence of hydrogen and metal impurities [32–34]. The complete recovery in the dark at near room temperature and the determined value of activation energy (0.656 eV, see below) evidenced the iron–boron pair-related LID in our case.

It is known that FeB pair dissociations in the SC base are accompanied by the change in lifetime of minority carriers τ . As an indicator of this quantity we considered short circuit current I_{SC} , which was measured under SC illumination by a low energy monochromatic light source. This was a light emitting diode (LED) with radiation power $P_{\text{ph}} \sim 350 \text{ } \mu\text{W}$ (measured by PowerMeter Rk-5720) and light wavelength $\lambda = 940 \text{ nm}$. As the calculations showed, under these conditions the level of nonequilibrium carrier excitations was $\Delta n < 10^{12} \text{ cm}^{-3}$.

The kinetics of short circuit current was measured after intensive illumination of the sample (see Fig. 2). All the measurements were carried out by varying the temperature from 300 to 340 K with a thermoelectric cooler, and by stabilizing it with a computer-controlled PID loop to better than 0.05 K.

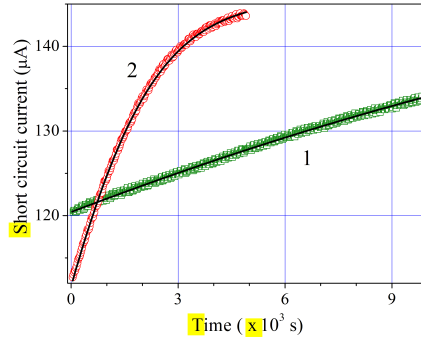


Fig. 2 Measured under low-intensive (LED) illumination short circuit current plotted as a function of the time after high-intensive (halogen lamp) illumination. The marks are the experimental results, the lines are the fitted curves using Eqs. (1)-(9). The zero of time corresponds to the moment of intensive illumination termination. T , K: 300 (1, green squares), 330 (2, red circles)

The SC temperature was controlled by STS-21 sensor, which was placed on the front sample surface.

The FeB pair association in the dark was accompanied by the τ increase and was monitored by measuring the I_{SC} under LED illumination. The LED illumination induced excess carrier density $< 10^{12} \text{ cm}^{-3}$, had duty cycle 0.5% while $I_{SC}(t)$ measuring, and did not cause FeB dissociation. Moreover, the fitting of the measured dependencies $I_{SC}(t)$ after high-intensive illumination allows determining the pair concentration and the characteristic time of the FeB complex formation. In fact, in conditions of homogeneous carrier generation in the base by the LED illumination, the short circuit current can be described as follows [35, 36]:

$$I_{SC}(t) = \frac{P_{ph}(1 - R_{ph})q\beta\lambda}{hc} \frac{\alpha_{ph}L_n(t)}{1 + \alpha_{ph}L_n(t)}, \quad (1)$$

where P_{ph} is the LED light power, λ is the light wavelength (940 nm), q is elementary charge, h is the Planck constant, c is the speed of light, $\alpha_{ph} = \alpha_{ph}(T, \lambda)$ is the coefficient of light absorption, which was calculated according to [37, 38], T is the cell temperature, R_{ph} is the coefficient of reflection; as shown by the calculations with using recurrent correlations for coefficients of amplitude reflections [39, 40], in our case from the silicon SC with two layered antireflection coating $R_{ph}(940 \text{ nm}) = 0.14$; β is the coefficient of quantum yield, $\beta = 1$; L_n is the diffusion length of minority carriers. As the measurements of L_n by spectral dependence of internal quantum yield show, the quantity was from 35 to 150 μm (for different samples), which justifies the usage of expression (1). In its turn

$$L_n(t) = \sqrt{\frac{\mu_n k T \tau(t)}{q}}, \quad (2)$$

where μ_n is the electron mobility, was calculated by Klaassen theory [41], k is the Boltzmann constant.

In the assumption that it is the iron related defects that play an essential role in the recombination, the following expression can be used to estimate τ according to Mattisen rule:

$$\tau(t)^{-1} = \tau_{rad}^{-1} + \tau_{Aug}^{-1} + (\tau_{SRH}^{Fe_i}(t))^{-1} + (\tau_{SRH}^{FeB}(t))^{-1} + \tau_{other}^{-1}, \quad (3)$$

where τ_{rad} is the lifetime associated with band-to-band radiation recombination

$$\tau_{rad}^{-1} = B(N_A + n_0 + \Delta n), \quad (4)$$

τ_{Aug} is the life time associated with Auger processes:

$$\tau_{Aug}^{-1} = C_p N_A^2, \quad (5)$$

the values of recombination coefficients B and C_p were calculated by data from [42, 43]; $n_0 = n_i^2/N_A$, n_i is the intrinsic carrier concentration, whose dependence on temperature was taken from [44]; $\tau_{SRH}^{Fe_i}$ and τ_{SRH}^{FeB} are related to the recombinations at interstitial iron atoms Fe_i and at FeB pairs, accordingly; τ_{other} describes the rest of recombination pathways including surface recombination.

In order to calculate $\tau_{SRH}^{Fe_i}$ and τ_{SRH}^{FeB} , Shockley–Read–Hall model was used:

$$\tau_{SRH}^{Fe_i, FeB}(t) = \frac{\tau_{p0}(t)(n_0 + n_1 + \Delta n) + \tau_{n0}(t)(N_A + p_1 + \Delta n)}{N_A + n_0 + \Delta n}, \quad (6)$$

where $\tau_{p0, n0}(t) = (N_{trap}(t)\sigma_{p,n}v_{th}^{p,n})^{-1}$, $N_{trap}(t)$ is the trap concentration (N_{Fe_i} and N_{FeB} for Fe_i and FeB, respectively), σ_n , σ_p are the cross sections of the recombination centers for electrons and holes, respectively, v_{th}^n , v_{th}^p are the average thermal velocities of electrons and holes calculated according to [45], $n_1 = N_C \exp(-(E_C - E_t)/kT)$, $p_1 = N_V \exp(-(E_t - E_V)/kT)$, N_C , N_V are the effective densities of states near the bottom of the conduction band and the top of the valence band, respectively [44], E_C , E_V are the energy positions of the bottom of the conduction band and the top of the valence band, E_t is the energy position of the recombination level due to defect. The parameters of recombination centers related to Fe_i and FeB were taken from [46].

The time dependence of interstitial iron atom concentration after pair dissociations is described by the known expression from [47]:

$$N_{Fe_i}(t) = (N_{Fe_i,0} - N_{Fe_i,eq}) \cdot \exp(-t/\tau_{ass}) + N_{Fe_i,eq}, \quad (7)$$

where τ_{ass} is the characteristic time of the formation of FeB pair, $N_{Fe_i,0}$ is the concentration of interstitial iron atoms formed due to high-intensive illumination, $N_{Fe_i,eq}$ is the part of interstitial iron atoms with $N_{Fe_i,0}$ that remain

unpaired in equilibrium state (after a long exposition in darkness)[27]:

$$N_{\text{Fe}_i, \text{eq}} = \frac{N_{\text{Fe}_i, 0}}{\left[1 + N_A 10^{-23} \exp\left(\frac{0.582 \text{ eV}}{kT}\right)\right] \left[1 + \exp\left(-\frac{E_F - 0.394 \text{ eV}}{kT}\right)\right]}, \quad (8)$$

E_F is the quasi-Fermi level.

In its turn, time dependence of iron-boron pair concentration N_{FeB} formed as a result of association of the part with $N_{\text{Fe}_i, 0}$ should be described by the expression

$$N_{\text{FeB}}(t) = N_{\text{Fe}_i, 0} - N_{\text{Fe}_i}(t). \quad (9)$$

We fitted experimentally measured dependencies of short circuit current according to the complex of the above equations (see the examples in Fig. 2). The fitting was performed by metaheuristic method EBLSHADE [48], the parameters to be found were P_{ph} , τ_{other} , $N_{\text{Fe}_i, 0}$, and τ_{ass} .

For the data given in Fig. 2, the parameters found by the fitting had the following values. $P_{ph} = (3.2 \pm 0.3) \times 10^{-4}$ W, which agrees well with the measured value.

In cases when the time of intensive illumination was over 20 s, $\tau_{other} > 100$ s, which testifies that the contribution of other recombination pathways can be neglected.

$N_{\text{Fe}_i, 0} = (7 \pm 1) \times 10^{12} \text{ cm}^{-3}$, which is on the one hand a rather typical value for solar silicon, on the other hand it is close to the values $3 \times 10^{12} \text{ cm}^{-3}$ obtained for the samples of the same series by the spectral dependence of intrinsic quantum efficiency method.

Finally, the values of τ_{ass} were found to be (1380 ± 20) s for $T = 330$ K and $(1.26 \pm 0.02) \times 10^4$ s for $T = 300$ K. It was reported that τ_{ass} should depend on boron concentration as well as temperature, in particular the following expression was proposed to estimate its value in [28]:

$$\tau_{ass} = \frac{5.7 \times 10^5 T}{N_A} \exp\left(\frac{E_m}{kT}\right), \quad (10)$$

where E_m is the energy of Fe_i migration. Being calculated by using Eq. (10) on the basis of the obtained values of association time, it comprised $E_m = (0.656 \pm 0.002)$ eV. This value coincides with the well known from [28, 49] value of 0.66 eV.

The coincidence of the obtained data with the expected ones proves that the investigations of short circuit current kinetics after intensive illumination can be applied in finding such parameters of defects related to iron as FeB pair association time and Fe_i initial concentration.

3 Results and Discussion

The experiments have shown that the US loading leads to speed up of recovery of short circuit current after high-intensive illumination. Therefore, the

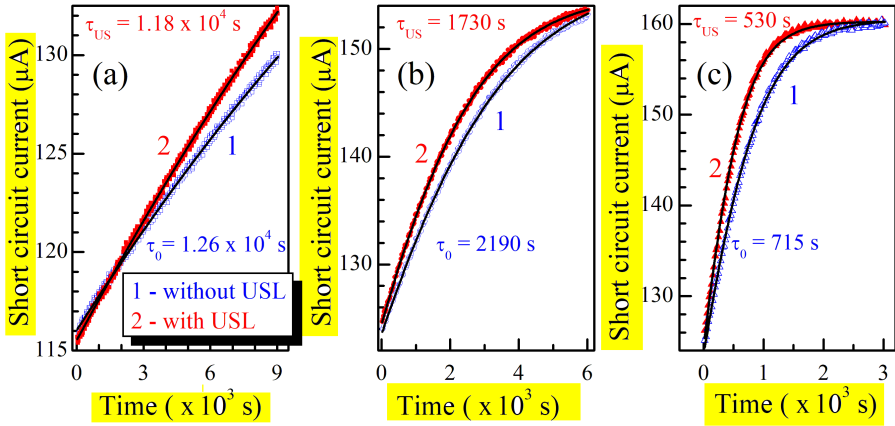


Fig. 3 Kinetics of short circuit current after intensive illumination under USL ($f_{US} = 2.4$ MHz, filled red marks on the chart) and without USL (empty green marks). Solid lines indicate fitting according to Eqs. (1)-(9). T , K: 300 (a), 320 (b), 340 (c)

FeB association is intensified under AW action. Fig. 3 shows, for example, the time dependencies of short circuit current after intensive illumination at different temperatures that were measured under USL as well as without USL. It is seen that the resumption speed I_{SC} depends both on temperature (which is quite expectable according to Eq. (10)) and on applied USL. The figure also shows τ_{ass} values which were found by nonlinear fitting of experimental curves. Here, we use τ_0 for the time of association without USL and τ_{US} for the conditions of USL. As seen from the figure, $\tau_{US}/\tau_0 < 1$. Further on, to characterize quantitatively the degree of acoustically induced (AI) decrease of association time, we shall use the quantity τ_{US}/τ_0 .

The investigations show that the degree at which the association accelerates under USL depends on acoustic wave intensity. Fig. 4 gives the data that evidence about decrease in τ_{US} due to increase in W_{US} . It is evident that whatever the US frequency is, τ_{US}/τ_0 practically linearly depends on the intensity at small values of W_{US} . As USL becomes more intense, the saturation of τ_{US} is observed, which corresponds to about $0.7\tau_0$.

Also, Fig. 4 demonstrates that the efficiency of AI change in migration energy decreases as the US frequency increases, this effect being observed for all the samples and does not depend on impurity iron concentration. In particular, saturation τ_{US}/τ_0 at $f_{US} = 2.4$ MHz is observed at approximately $W_{US} = 0.6$ W/cm², while for 9.0 MHz it is revealed at 0.9 W/cm², see Fig. 4(b). As for the saturation magnitude, it does not depend on f_{US} . Transverse waves, despite lower frequency, more weakly impact the processes of FeB pair association. It is previously shown [26] that the acoustically-induced change of complex defect parameters can be attributed to the variation in the distance of the components, and this effect is intensified in the case of the transverse waves. The opposite feature of investigated phenomenon testifies that the AI

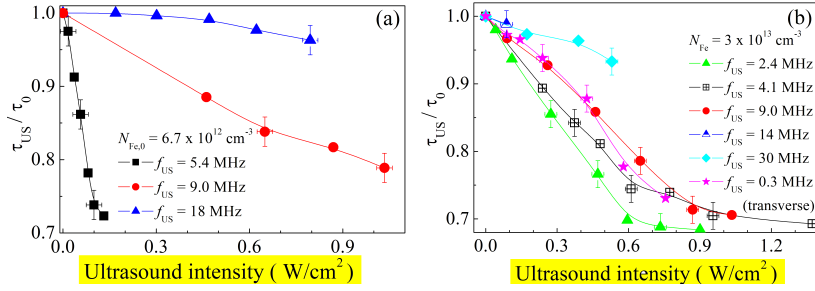


Fig. 4 The dependencies of the degree of AI time decrease on the applied US intensity at different f_{US} . Parts a and b present the samples with different iron concentrations. $T = 340$ K. The marks are the experimental results, the lines are given for convenience only

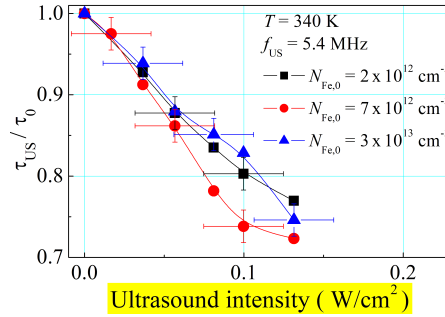


Fig. 5 The dependencies of the degree of AI association time decrease on applied US intensity in SC with different content of iron atoms. $T = 340$ K. $f_{US} = 5.4$ MHz. The marks are the experimental results, the lines are given for convenience only

acceleration of the FeB pair association does not deal with iron-boron distance change.

Fig. 4 also gives iron concentrations $N_{Fe,0}$ obtained from I_{SC} relaxation in conditions of complete pair dissociation (i.e. the illumination that causes the maximum short circuit current decrease). The next figure, Fig. 5, presents τ_{US}/τ_0 dependencies for the samples with different iron concentrations under USL of the same US frequency. It is evident that the magnitude of AI effect in fact does not depend on $N_{Fe,0}$.

Our experiments have shown that as the temperature decreases the efficiency of US impact on τ_{ass} increases (see Fig. 6 which presents the temperature dependence of τ_{US}/τ_0) at a constant intensity of US application. In general, these curves are close to linear.

The association of FeB complex happens at the expense of Fe_i diffusion towards the boron atoms located in substituting positions and strongly bound with the neighbour due to forming covalent bonds with them. Therefore, the τ_{ass} depends on the coefficient of iron diffusion D_{Fe} , so a more detailed, in

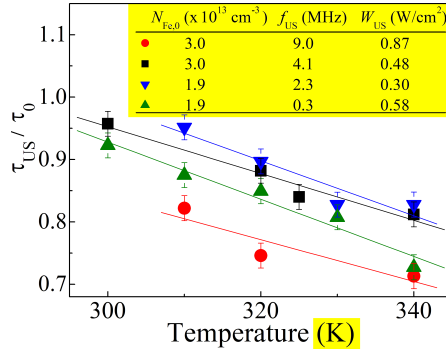


Fig. 6 Temperature dependencies of acoustically induced FeB association time decrease. The marks are the experimental results, the lines are the linear fitted curves

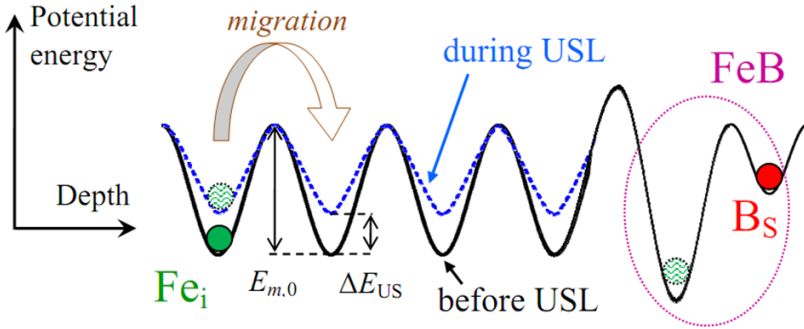


Fig. 7 A schematic picture showing the spatial variation of the potential energy of iron interstitial atom in Si as a function of position near the boron substitutional atom. US stress lowers the energy barrier for Fe migration. The curves are scaled arbitrarily

comparison with Eq. (10), expression takes the following form [28, 30, 50]:

$$\tau_{ass} = \frac{\varepsilon \varepsilon_0 k T}{q^2 D_{Fe} N_A} = \frac{\varepsilon \varepsilon_0 k T}{q^2 D_{0,Fe} N_A} \exp\left(\frac{E_m}{kT}\right), \quad (11)$$

where $D_{Fe} = D_{0,Fe} \exp(-E_m/kT)$, $D_{0,Fe}$ is a temperature-independent multiplier, in the general case [51–53] $D_{0,Fe} = \beta \nu a^2 \exp(\delta S_{Fe}/k)$, β is a correlation factor, ν is an effective vibrational (attempt) frequency, a is a jump distance, δS_{Fe} is the migration entropy.

As evident from Eq. (11), the decrease in FeB association time under USL testifies about AI increase in D_{Fe} . It is, most probable, due to the increase in diffusion energy (see Fig. 7). Enhanced diffusion of impurities in the US field was observed previously both in poly- and mono-crystals of silicon and gallium arsenide [54, 55]. The decrease in interstitial iron atom migration energy can be given as

$$E_m \xrightarrow{\text{ultrasound}} E_{m,0} - \Delta E_{US}, \quad (12)$$

where $E_{m,0}$ is the migration energy without elastic oscillations in silicon SC, which is $E_{m,0} \sim 0.66$ eV according to [28, 49] and our experimental data; ΔE_{US} is the AI change in this quantity value. According to the performed investigations $\Delta E_{US} = f(W_{US}, f_{US}, T)$ and does not exceed 10 meV.

The physics of the found AI effect can be the following. By using thermodynamic formalism it was shown in [51] that the ability of impurities in Si to diffuse depends on mechanical stress η :

$$\frac{D(\eta)}{D(0)} = \exp\left(\frac{\eta V^*}{kT}\right) = \exp\left(\frac{\eta[-\Omega + V^r + V^m]}{kT}\right), \quad (13)$$

where V^* is an activation strain tensor, Ω is the atomic volume representing crystal dimension changes upon the formation of lattice site before the lattice relaxation around the newly created point defect is permitted, V^r is a relaxation volume, V^m is a migration strain tensor, which characterizes stress impact on the defect mobility. The enhance Fe_i diffusivity in the strain field is discussed in [56] as well.

In our opinion, this is the mechanism, which explains the found US impact on FeB pairs association in silicon SC. As seen from Eq. (13), the diffusion coefficient change caused by the applied stress is thermally activated, which explains the observed temperature dependence of AI changes in τ_{ass} . In addition, generally V^* contains 81 component [51], and therefore change in D depends on the direction of atom elastic displacements. This accounts for less effective AI impact of transverse waves. It should be noted, that it is the absorption of oscillation energy that the authors [57, 58] use to reveal the causes of USL impact on defect system in Si–SiO₂ structures, and in particular AI increase in impurities mobility.

The observation reported here opens up new possibilities in manipulating electronic properties of silicon barrier devices. For example, as mentioned above, during phosphor diffusion, the iron impurity gettering occurs as well. This happens at high temperatures (near 900°C), and for this reason iron is found in unpaired interstitial state. USL applied during this technological process should increase the degree of the SC basic region cleaning due to AI increase in Fe coefficient and as a result improve SC performance.

4 Conclusion

The ultrasound influence on FeB pair association in silicon solar cells has been investigated experimentally. The investigation has revealed that pair associations are accelerated due to enhance of iron atom diffusion under the action of ultrasound field. The effect gets stronger with the increase in temperature and decrease in USL frequency. The application of longitudinal waves is more effective than that of transverse waves. The effect can be related to a nearly room-temperature decrease in iron migration energy (to 10 meV) in the ultrasound stress fields. Thus, ultrasound can be an effective functional tool for controlling silicon structure characteristics.

Statements and Declarations

Conflict of interest. There are no conflicts to declare.

Data availability statement. Some or all data generated or used during the study are available from the corresponding author by request.

Funding. This work was supported by National Research Foundation of Ukraine (project number 2020.02/0036).

Author Contributions. All authors contributed equally to this work.

References

- [1] Ostapenko, S.S., Korsunskaya, N.E., Sheinkman, M.K.: Ultrasound stimulated defect reactions in semiconductors. In: Defect Interaction and Clustering in Semiconductors. Solid State Phenomena, vol. 85–86, pp. 317–336. Trans Tech Publications Ltd, Zürich (2002). <https://doi.org/10.4028/www.scientific.net/SSP.85-86.317>
- [2] Savkina, R.K.: Recent progress in semiconductor properties engineering by ultrasonication. Recent Patents on Electrical & Electronic Engineering **6**(3), 157–172 (2013). <https://doi.org/10.2174/22131116113066660008>
- [3] Olikh, O.Y., Gorb, A.M., Chupryna, R.G., Pristay–Fenenkov, O.V.: Acousto–defect interaction in irradiated and non–irradiated silicon n^+p structure. J. Appl. Phys. **123**(16), 161573 (2018). <https://doi.org/10.1063/1.5001123>
- [4] Davletova, A., Karazhanov, S.Z.: Open-circuit voltage decay transient in dislocation-engineered Si p–n junction. Journal of Physics D: Applied Physics **41**(16), 165107 (2008). <https://doi.org/10.1088/0022-3727/41/16/165107>
- [5] Olikh, Y., Tymochko, M., Olikh, O.: Mechanisms of two-stage conductivity relaxation in cdt:cl with ultrasound. J. Electron. Mater. **49**(8), 4524–453 (2020). <https://doi.org/10.1007/s11664-020-08179-7>
- [6] Olikh, O.: Reversible influence of ultrasound on γ –irradiated Mo/n-Si Schottky barrier structure. Ultrasonics **56**, 545–550 (2015). <https://doi.org/10.1016/j.ultras.2014.10.008>
- [7] Olikh, O.Y., Voytenko, K.V., Burbelo, R.M.: Ultrasound influence on I–V–T characteristics of silicon Schottky barrier structure. J. Appl. Phys. **117**(4), 044505 (2015). <https://doi.org/10.1063/1.4906844>
- [8] Sukach, A.V., Teterkin, V.V.: Ultrasonic treatment–induced modification of the electrical properties of InAs p–n junctions. Tech. Phys. Lett. **35**(6), 514–517 (2009). <https://doi.org/10.1134/S1063785009060108>

- [9] Krüger, D., Romanyuk, B., Melnik, V., Olikh, Y., Kurps, R.: Influence of in situ ultrasound treatment during ion implantation on amorphization and junction formation in silicon. *J. Vac. Sci. Technol. B* **20**(4), 1448–1451 (2002). <https://doi.org/10.1116/1.1493784>
- [10] Romanyuk, B., Melnik, V., Olikh, Y., Popov, V., Krüger, D.: Modification of the si amorphization process by in situ ultrasonic treatment during ion implantation. *Semicond. Sci. Technol.* **16**(5), 397–401 (2001). <https://doi.org/10.1088/0268-1242/16/5/320>
- [11] Kalem, S., Yavuzcetin, O., Altineller, C.: Effect of light exposure and ultrasound on the formation of porous silicon. *Journal of Porous Materials* **7**(1), 381–383 (2000). <https://doi.org/10.1023/A:1009687021287>
- [12] Fujita, S., Kaneko, K., Ikenoue, T., Kawaharamura, T., Furuta, M.: Ultrasonic-assisted mist chemical vapor deposition of ii-oxide and related oxide compounds. *Phys. Status Solidi C* **11**(7–8), 1225–1228 (2014). <https://doi.org/10.1002/pssc.201300655>
- [13] Istratov, A.A., Hieslmair, H., Weber, E.R.: Iron and its complexes in silicon. *Applied Physics A: Materials Science & Processing* **69**(1), 13–44 (1999). <https://doi.org/10.1007/s003390050968>
- [14] Schubert, M.C., Padilla, M., Michl, B., Mundt, L., Giesecke, J., Hohl-Ebinger, J., Benick, J., Warta, W., Tajima, M., Ogura, A.: Iron related solar cell instability: Imaging analysis and impact on cell performance. *Sol. Energy Mater. Sol. Cells* **138**, 96–101 (2015). <https://doi.org/10.1016/j.solmat.2015.03.001>
- [15] Laine, H.S., Vähänissi, V., Morishige, A.E., Hofstetter, J., Haarahiltunen, A., Lai, B., Savin, H., Fenning, D.P.: Impact of iron precipitation on phosphorus-implanted silicon solar cells. *IEEE Journal of Photovoltaics* **6**(5), 1094–1102 (2016). <https://doi.org/10.1109/JPHOTOV.2016.2576680>
- [16] Vähänissi, V., Haarahiltunen, A., Talvitie, H., Yli-Koski, M., Savin, H.: Impact of phosphorus gettering parameters and initial iron level on silicon solar cell properties. *Progress in Photovoltaics: Research and Applications* **21**(5), 1127–1135 (2013). <https://doi.org/10.1002/pip.2215>
- [17] Mchedlidze, T., Möller, C., Lauer, K., Weber, J.: Evolution of iron-containing defects during processing of si solar cells. *J. Appl. Phys.* **116**(24), 245701 (2014). <https://doi.org/10.1063/1.4905027>
- [18] Bartel, T., Gibaja, F., Graf, O., Gross, D., Kaes, M., Heuer, M., Kirscht, F., Möller, C., Lauer, K.: Dynamics of iron-acceptor-pair formation in co-doped silicon. *Appl. Phys. Lett.* **103**(20), 202109 (2013). <https://doi.org/>

10.1063/1.4830227

- [19] Ajayan, J., Nirmal, D., Mohankumar, P., Saravanan, M., Jagadesh, M., Arivazhagan, L.: A review of photovoltaic performance of organic/inorganic solar cells for future renewable and sustainable energy technologies. *Superlattices Microstruct.* **143**, 106549 (2020). <https://doi.org/10.1016/j.spmi.2020.106549>
- [20] Green, M.A.: Photovoltaic technology and visions for the future. *Prog. Energy* **1**(1), 013001 (2019). <https://doi.org/10.1088/2516-1083/ab0fa8>
- [21] Ostapenko, S.S., Jastrzebski, L., Lagowski, J., Sopori, B.: Increasing short minority carrier diffusion lengths in solar-grade polycrystalline silicon by ultrasound treatment. *Appl. Phys. Lett.* **65**(12), 1555–1557 (1994). <https://doi.org/10.1063/1.112942>
- [22] Ostapenko, S.S., Bell, R.E.: Ultrasound stimulated dissociation of Fe–B pairs in silicon. *J. Appl. Phys.* **77**(10), 5458–5460 (1995). <https://doi.org/10.1063/1.359243>
- [23] Brailsford, A.D.: Abrupt-kink model of dislocation motion. *Phys. Rev.* **122**(3), 778–786 (1961). <https://doi.org/10.1103/PhysRev.122.778>
- [24] Pavlovich, V.N.: Enhanced diffusion of impurities and defects in crystals in conditions of ultrasonic and radiative excitation of the crystal lattice. *Phys. Status Solidi B* **180**(1), 97–105 (1993). <https://doi.org/10.1002/pssb.2221800108>
- [25] Peleshchak, R.M., Kuzyk, O.V., Dan’kiv, O.O.: Formation of periodic structures under the influence of an acoustic wave in semiconductors with a two-component defect subsystem. *Ukr. J. Phys.* **61**(8), 741–746 (2016). <https://doi.org/10.15407/ujpe61.08.0741>
- [26] Olikh, O.Y.: Acoustically driven degradation in single crystalline silicon solar cell. *Superlattices Microstruct.* **117**, 173–188 (2018). <https://doi.org/10.1016/j.spmi.2018.03.027>
- [27] Wijaranakula, W.: The reaction kinetics of iron–boron pair formation and dissociation in p-type silicon. *J. Electrochem. Soc.* **140**(1), 275–281 (1993). <https://doi.org/10.1149/1.2056102>
- [28] Möller, C., Bartel, T., Gibaja, F., Lauer, K.: Iron-boron pairing kinetics in illuminated p-type and in boron/phosphorus co-doped n-type silicon. *J. Appl. Phys.* **116**(2), 024503 (2014). <https://doi.org/10.1063/1.4889817>
- [29] Tan, J., Macdonald, D., Rougieux, F., Cuevas, A.: Accurate measurement of the formation rate of iron–boron pairs in silicon. *Semicond Sci. Technol.*

- 26**(5), 055019 (2011). <https://doi.org/10.1088/0268-1242/26/5/055019>
- [30] Macdonald, D., Roth, T., Deenapanray, P.N.K., Bothe, K., Pohl, P., Schmidt, J.: Formation rates of iron-acceptor pairs in crystalline silicon. *J. Appl. Phys.* **98**(8), 083509 (2005). <https://doi.org/10.1063/1.2102071>
- [31] Lindroos, J., Savin, H.: Review of light-induced degradation in crystalline silicon solar cells. *Sol. Energy Mater. Sol. Cells* **147**, 115–126 (2016). <https://doi.org/10.1016/j.solmat.2015.11.047>
- [32] Schmid, A., Fischer, C., Skorka, D., Herguth, A., Winter, C., Zuschlag, A., Hahn, G.: On the role of AlO_x thickness in AlO_x/SiN_y: H layer stacks regarding light- and elevated temperature-induced degradation and hydrogen diffusion in c-Si. *IEEE Journal of Photovoltaics* **11**(4), 967–973 (2021). <https://doi.org/10.1109/JPHOTOV.2021.3075850>
- [33] Wagner, M., Wolny, F., Hentsche, M., Krause, A., Sylla, L., Kropfgans, F., Ernst, M., Zierer, R., Bönsch, P., Müller, P., Schmidt, N., Osinniy, V., Hartmann, H.-P., Mehnert, R., Neuhaus, H.: Correlation of the LeTID amplitude to the Aluminium bulk concentration and Oxygen precipitation in PERC solar cells. *Sol. Energy Mater. Sol. Cells* **187**, 176–188 (2018). <https://doi.org/10.1016/j.solmat.2018.06.009>
- [34] Chen, D., Kim, M., Stefani, B.V., Hallam, B.J., Abbott, M.D., Chan, C.E., Chen, R., Payne, D.N.R., Nampalli, N., Ciesla, A., Fung, T.H., Kim, K., Wenham, S.R.: Evidence of an identical firing-activated carrier-induced defect in monocrystalline and multicrystalline silicon. *Sol. Energy Mater. Sol. Cells* **172**, 293–300 (2017). <https://doi.org/10.1016/j.solmat.2017.08.003>
- [35] Fahrenbruch, A., Bube, R.: *Fundamentals of Solar Cells: Photovoltaic Solar Energy Conversion*, p. 580. Academic Press, NY, London, Paris (1983)
- [36] Razeghi, M., Rogalski, A.: Semiconductor ultraviolet detectors. *J. Appl. Phys.* **79**(10), 7433–7473 (1996). <https://doi.org/10.1063/1.362677>
- [37] Rajkanan, K., Singh, R., Shewchun, J.: Absorption coefficient of silicon for solar cell calculations. *Solid-State Electron.* **22**(9), 793–795 (1979). [https://doi.org/10.1016/0038-1101\(79\)90128-X](https://doi.org/10.1016/0038-1101(79)90128-X)
- [38] Green, M.A., Keevers, M.J.: Optical properties of intrinsic silicon at 300 k. *Progress in Photovoltaics: Research and Applications* **3**(3), 189–192 (1995). <https://doi.org/10.1002/pip.4670030303>
- [39] Klyui, N.I., Kostilyov, V.P., Rozhin, A.G., Gorbulik, V.I., Litovchenko, V.G., Voronkin, M.A., Zaika, N.I.: Silicon solar cells with antireflecting

- and protective coatings based on diamond-like carbon and silicon carbide films. *Opto-Electr. Rev.* **8**(4), 402–405 (2000)
- [40] Litovchenko, V.G., Klyui, N.I., Kostylyov, V.P., Gorbulik, V.I., Piryatinskii, Y.P.: Nitrogen containing diamond-like carbon films as protective and fluorescent layers for silicon solar cells. *Opto-Electr. Rev.* **8**(4), 406–409 (2000)
 - [41] Klaassen, D.B.M.: A unified mobility model for device simulation — I. model equations and concentration dependence. *Solid-State Electron.* **35**(7), 953–959 (1992). [https://doi.org/10.1016/0038-1101\(92\)90325-7](https://doi.org/10.1016/0038-1101(92)90325-7)
 - [42] Nguyen, H.T., Baker–Finch, S.C., Macdonald, D.: Temperature dependence of the radiative recombination coefficient in crystalline silicon from spectral photoluminescence. *Appl. Phys. Lett.* **104**(11), 112105 (2014). <https://doi.org/10.1063/1.4869295>
 - [43] Altermatt, P.P., Schmidt, J., Heiser, G., Aberle, A.G.: Assessment and parameterisation of Coulomb–enhanced Auger recombination coefficients in lowly injected crystalline silicon. *J. Appl. Phys.* **82**(10), 4938–4944 (1997). <https://doi.org/10.1063/1.366360>
 - [44] Couderc, R., Amara, M., Lemiti, M.: Reassessment of the intrinsic carrier density temperature dependence in crystalline silicon. *J. Appl. Phys.* **115**(9), 093705 (2014). <https://doi.org/10.1063/1.4867776>
 - [45] Green, M.A.: Intrinsic concentration, effective densities of states, and effective mass in silicon. *J. Appl. Phys.* **67**(6), 2944–2954 (1990). <https://doi.org/10.1063/1.345414>
 - [46] Rougieux, F.E., Sun, C., Macdonald, D.: Determining the charge states and capture mechanisms of defects in silicon through accurate recombination analyses: A review. *Sol. Energy Mater. Sol. Cells* **187**, 263–272 (2018). <https://doi.org/10.1016/j.solmat.2018.07.029>
 - [47] Murphy, J.D., Bothe, K., Olmo, M., Voronkov, V.V., Falster, R.J.: The effect of oxide precipitates on minority carrier lifetime in p–type silicon. *J. Appl. Phys.* **110**(5), 053713 (2011). <https://doi.org/10.1063/1.3632067>
 - [48] Mohamed, A.W., Hadi, A.A., Jambi, K.M.: Novel mutation strategy for enhancing SHADE and LSHADE algorithms for global numerical optimization. *Swarm Evol. Comput.* **50**, 100455 (2019). <https://doi.org/10.1016/j.swevo.2018.10.006>
 - [49] Macdonald, D., Cuevas, A., Geerligs, L.J.: Measuring dopant concentrations in compensated p–type crystalline silicon via iron–acceptor pairing. *Appl. Phys. Lett.* **92**(20), 202119 (2008). <https://doi.org/10.1063/1.2998888>

1063/1.2936840

- [50] Khelifati, N., Laine, H.S., Vähänissi, V., Savin, H., Bouamama, F.Z., Bouhafs, D.: Dissociation and formation kinetics of iron–boron pairs in silicon after phosphorus implantation gettering. *Phys Status Solidi A* **216**(17), 1900253 (2019). <https://doi.org/10.1002/pssa.201900253>
- [51] Aziz, M.J.: Stress effects on defects and dopant diffusion in Si. *Mater. Sci. Semicond. Process.* **4**(5), 397–403 (2001). [https://doi.org/10.1016/S1369-8001\(01\)00014-2](https://doi.org/10.1016/S1369-8001(01)00014-2)
- [52] Stavola, M. (ed.): *Identification of Defects in Semiconductors*. Academic Press, San Diego, Ca (1998)
- [53] Weber, E.R.: Transition metals in silicon. *Appl. Phys. A* **30**(1), 1–22 (1983). <https://doi.org/10.1007/BF00617708>
- [54] Ostapenko, S.: Defect passivation using ultrasound treatment: fundamentals and application. *Applied Physics A: Materials Science & Processing* **69**(2), 225–232 (1999). <https://doi.org/10.1007/s003390050994>
- [55] Zaveryukhin, B.N., Zaveryukhina, N.N., Tursunkulov, O.M.: Variation of the reflection coefficient of semiconductors in a wavelength range from 0.2 to 20 μm under the action of ultrasonic waves. *Tech. Phys. Lett.* **28**(9), 752–756 (2002). <https://doi.org/10.1134/1.1511774>
- [56] Ziebarth, B., Mrovec, M., Elsässer, C., Gumbsch, P.: Influence of dislocation strain fields on the diffusion of interstitial iron impurities in silicon. *Phys. Rev. B* **92**, 115309 (2015). <https://doi.org/10.1103/PhysRevB.92.115309>
- [57] Gorb, A.M., Korotchenkov, O.A., Olikh, O.Y., Podolian, A.O., Chupryna, R.G.: Influence of γ -irradiation and ultrasound treatment on current mechanism in au-sio₂-si structure. *Solid-State Electron.* **165**, 107712 (2020). <https://doi.org/10.1016/j.sse.2019.107712>
- [58] Kropman, D., Seeman, V., Dolgov, S., Medvids, A.: Effect of ultrasonic treatment on the defect structure of the Si–SiO₂ system. *Phys. Status Solidi C* **13**(10–12), 793–797 (2016). <https://doi.org/10.1002/pssc.201600052>